RSC Advances

PAPER

View Article Online
View Journal | View Issue

Cite this: *RSC Adv.*, 2017, **7**, 7906

Composition-controlled synthesis of $Ni_{2-x}Co_xP$ nanocrystals as bifunctional catalysts for water splitting†

Qingshuang Liang, Keke Huang, Xiaofeng Wu, Xiyang Wang, Wei Ma and Shouhua Feng*

Received 12th November 2016
Accepted 7th January 2017

DOI: 10.1039/c6ra26691f

www.rsc.org/advances

$Ni_{2-x}Co_xP$ ($0 \leq x \leq 2$) nanocrystals (NCs) with good control of composition are synthesized by a facile economical approach. Low-cost air-stable triphenylphosphine is used as phosphorus source and $NaBH_4$ is added to facilitate the reaction, which helps to carry out the reaction at relatively low temperature (250 °C). By modulating the Ni/Co precursor ratios, the composition of $Ni_{2-x}Co_xP$ NCs can be tuned over the whole range. A comprehensive study of the key role of $NaBH_4$ on the metal phosphide NCs formation reveals that $NaBH_4$ can efficiently activate the triphenylphosphine, lowering the thermodynamic barrier for the P–C bond broken and thus reducing the reaction temperature. As-prepared $Ni_{2-x}Co_xP$ NCs show Ni/Co-composition dependent catalytic performance on both hydrogen evolution reaction (HER) and oxygen evolution reaction (OER). In particular, OER catalytic activities follow the volcano relationship due to the synergistic effect. The $Ni_{1.0}Co_{1.0}P$ NCs exhibit the highest OER catalytic activity with the overpotential of 0.34 V at a current density of 10 mA cm^{-2}, among the top tier of water oxidation catalysts. In addition to providing a new green low-cost route to composition controllable synthesis of ternary phosphides, this work also contributes to fundamental guideline on rational design of low-cost high-efficient catalysts for water splitting.

1. Introduction

Electrochemical water splitting offers a promising strategy for renewable energy storage.[1] The two half reactions of water splitting, the hydrogen evolution reaction (HER) and the oxygen evolution reaction (OER), both require high performance electrocatalysts to facilitate. The development of efficient and low-cost electrocatalysts is highly desirable.[2–4] While significant advance has been made in this area, the currently prevalent strategies often result in incompatible integration of catalyzing both HER and OER in the same electrolyte.[5–7] Only a few catalysts have been reported to be capable of catalyzing both HER and OER in the same media.[8–10] The development of bifunctional HER and OER catalysts is attractive for water splitting device since it has advantages of simplifying the electrolyzer system and lowing the overall cost.

Transition metal phosphides have been extensively studied as low cost highly active catalysts for HER in the last few years.[11–19] Especially, some binary phosphides, such as CoP, Ni_2P, have been found to be active catalysts for both HER and OER recently.[9,10,20–25] Hu *et al.* report the bifunctional catalytic properties of Ni_2P for water splitting in alkaline conditions.[10] The activity for OER comes from the core–shell Ni_2P/NiO_x assembly generated *in situ* under catalytic conditions. Analogous behavior is reported by Sun *et al.* for hierarchically porous urchin-like Ni_2P superstructures anchored on nickel foam.[20] Li and co-workers show that a kind of hollow polyhedral cobalt phosphide is efficient bifunctional electrocatalysts for HER and OER.[21] Yoo *et al.* have observed the *in situ* transformation of hydrogen-evolving CoP nanoparticles toward efficient oxygen evolution catalysts.[9] While binary phosphides for bifunctional electrocatalysts have been explored, further improvement of the catalytic performances might be expected on the ternary phosphides due to the synergistic effect. By a combined experimental–theoretical approach, Jaramillo *et al.* find that the catalytic performances of transition metal phosphides for HER follow a volcano relationship.[26] They synthesized several mixtures of Co and Fe phosphides alloys and confirm that $Fe_{0.5}Co_{0.5}P$ exhibit the highest HER activity. Sun and co-worker have also reported that sea urchin-like $(Fe_{0.54}Co_{0.46})_2P$ is more efficient than either Co_2P or Fe_2P for OER.[27] Although these studies point the potential of ternary phosphides as more active catalysts, synergistic effect on bifunctional electrocatalyst has not been reported. Systematically study of composition dependent catalytic performance for water splitting is limited. The lack of synthetic methods that enable controllable tuning the

State Key Laboratory of Inorganic Synthesis and Preparative Chemistry, College of Chemistry, Jilin University, Changchun 130012, P. R. China. E-mail: shfeng@jlu.edu.cn; Fax: +86-431-85168624; Tel: +86-431-85168661

† Electronic supplementary information (ESI) available. See DOI: 10.1039/c6ra26691f

composition in a wide range impedes the clear understanding of the trends in intrinsic activities.

Various methods have been attempted to synthesize transition metal phosphides NCs, such as solvothermal synthesis, the reduction of phosphates and phosphinates, and microwave synthesis.[28–31] Whereas, these methods are complicated, and it is difficult to realize the component controllable synthesis of ternary phosphides NCs. Solution phase decomposition of a metal precursor in the presence of trioctylphosphine is the most promising method due to its excellent ability to control the size, shape, and composition.[32–34] However, the high price and instability of trioctylphosphine (TOP) as well as high temperatures (≥320 °C) needed for phosphidation limited the applications. Alternative and simpler methods are desirable to prepare component controllable ternary phosphides nanoparticles for a structure–activity study and further potential applications.

In this work, a green novel one-pot protocol to synthesize phase-pure component controllable $Ni_{2-x}Co_xP$ NCs ($0 \leq x \leq 2$) is developed. Low-cost air-stable triphenylphosphine (PPh_3) is used as phosphorus source and certain amounts of $NaBH_4$ are added to facilitate the reaction, which helps to carry out the reaction at relatively low temperature (250 °C). The composition of the $Ni_{2-x}Co_xP$ NCs can be tuned across the x range from 0 to 2 by modulating the molar ratio of the Ni/Co precursors. A comprehensive study of the key role of $NaBH_4$ on the metal phosphide NCs formation and growth is conducted. Composition dependent catalytic performance on both HER and OER is investigated and synergistic effect on the OER catalyst is found. In addition to providing a new green low-cost route to composition controllable synthesis of ternary phosphides, this work also contributes to fundamental guideline on rational design of improved catalysts for water splitting. This low temperature, facile and economical route to composition controllable multicomponent metal phosphides is expected to have broad applicability.

2. Experimental section

2.1 Materials

Triphenylphosphine (PPh_3, 99%) and oleylamine (OAm, 80–90%) were obtained from Aladdin. Hexane (analytical reagent), 2-propanol (analytical reagent), and $NaBH_4$ (96%) were purchased from Sinopharm Chemical Reagent Co., Ltd. Ethanol (analytical reagent), nickel(II) acetate tetrahydrate ($Ni(OAc)_2 \cdot 4H_2O$, 98%), and cobalt(II) acetate tetrahydrate ($Co(OAc)_2 \cdot 4H_2O$, 98%) were obtained from Beijing chemical works. All chemicals were used as received without further purification.

2.2 Synthesis of $Ni_{2-x}Co_xP$ nanoparticle ($0 \leq x \leq 2$)

In a typical synthesis process, 0.5 mmol $Ni(OAc)_2 \cdot 4H_2O$ (0.1245 g), 0.5 mmol $Co(OAc)_2 \cdot 4H_2O$ (0.1249 g), 3 mmol $NaBH_4$ (0.1135 g) and 2 mmol PPh_3 (0.5246 g) were loaded to a 100 mL three-neck flask attached with a Schlenk line. Then, 15 mL oleylamine were added. The mixed solution was degassed at 110 °C for 30 min with stirring and purged with argon three times. The temperature is then rapidly raised to 250 °C and held at 250 °C for 2 h with continuous vigorous stirring. After the mixture was cooled to room temperature, 5 mL of hexane and 25 mL of ethanol were added, and the mixture was sonicated for 5 min to remove all the free ligands and the unreacted precursors. The solution was centrifuged at 8000 rpm for 5 min. The upper layer liquid was decanted, and the isolated solid was dispersed in hexane and reprecipitated by adding ethanol. The centrifugation and precipitation procedure was repeated three times and the final products were redispersed in hexane or dried under vacuum for further measurements.

2.3 Characterization

X-ray power diffraction (XRD) patterns were recorded on a Rigaku D/Max 2500 V/PC X-ray diffractometer with graphite monochromated Cu Kα radiation ($\lambda = 0.1518$ nm). Transmission electron microscopy (TEM) and high-resolution transmission electron microscopy (HRTEM) images were taken with a FEI Tecnai G2 S-Twin F20 with an accelerating voltage of 200 kV. The sample for TEM analysis was prepared by placing a drop of the nanocrystals hexane solution on a carbon-coated copper grid and letting it dry in air. The compositions of the as-prepared $Ni_{2-x}Co_xP$ nanocrystals were determined quasi-quantitatively by a Helios NanoLab 600I from FEI Company, at an acceleration voltage of 20 kV. X-ray photoelectron spectroscopy (XPS) was carried out with Thermo ESCALab 250 analyzer operating at constant analyzer energy mode.

2.4 Electrochemical measurements

Before the electrochemical measurements, the samples were annealed in flowing H_2 (5%)/Ar (95%) at 450 °C for 30 min to remove the organic ligands that capped the surface of the $Ni_{2-x}Co_xP$ nanocrystals. The as-prepared catalysts (5 mg), Vulcan carbon black (VB, 1 mg) and Nafion solution (80 μL, 5 wt%) were dissolved in 0.5 mL 2-propanol and sonicated for 30 min to form a slurry. Then 20 μL of the slurry was loaded onto the surface of a glassy carbon electrode (GCE, 5 mm in diameter) and the electrode was dried at room temperature. The electrochemical measurements were carried out using a CHI 750D electrochemical workstation (CH Instruments, Inc., Shanghai) in a standard three-electrode setup. A saturated calomel electrode (SCE) was used as reference electrode and a Pt electrode as counter electrode. The electrocatalytic activities of the samples towards both HER and OER were examined by obtaining polarization curves using linear sweep voltammetry (LSV) with a scan rate of 10 mV s^{-1} at room temperature in 1.0 M KOH solution (pH ~ 13.6). There were several IR drops applied for compensation and no stirring were used for the linear sweep voltammetry. All the potentials reported in this paper were converted to the reversible hydrogen electrode (RHE).

3. Result and discussion

3.1 Synthesis of $Ni_{2-x}Co_xP$ nanoparticles

Solution thermal decomposition of metal–phosphine complexes is the most commonly used method to prepared metal

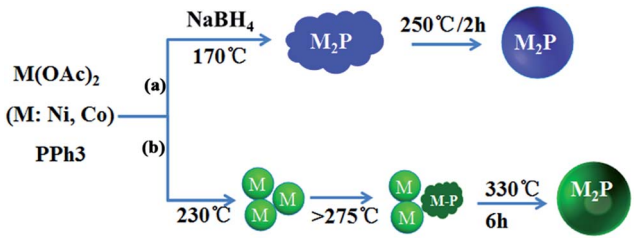

Scheme 1 Formation pathways for the as-prepared $Ni_{2-x}Co_xP$ NCs (a) with and (b) without the addition of $NaBH_4$.

phosphide NCs. Formation of metal phosphide NCs generally goes through a metal phase to metal phosphide transformation (Scheme 1b).[35–37] Due to the strong binding of P–C bond, high temperature (≥320 °C) is need for the broken of P–C bond and formation of metal–P bond.[32] Here in our ternary $Ni_{2-x}Co_xP$ nanoparticle synthesis, the needed reaction temperature can significantly decreased to 250 °C by adding certain amount of $NaBH_4$. Commercially available, low-coat, air-stable triphenylphosphine (PPh_3) was used as phosphorus source and $Ni(OAc)_2$ and $Co(OAc)_2$ were the metal precursors. With simply change the Ni/Co precursor ratios, composition tuning $Ni_{2-x}Co_xP$ nanoparticles were obtained.

The role of $NaBH_4$ on synthesis of $Ni_{2-x}Co_xP$ nanoparticles. With the adding of 3 mmol $NaBH_4$, phase-pure Ni_2P NCs were obtained after the reaction at 250 °C for 2 h (Fig. 1), while mixture of Ni and $Ni_{12}P_5$ NCs were found for the reaction without $NaBH_4$ (Fig. S1, ESI†). These results indicate that $NaBH_4$ is significantly important to carry out the reaction at relatively low temperature. Without the addition of $NaBH_4$, it was observed that the solution color changed from green to black at 230 °C, indicating that the Ni precursor was reduced to Ni phase by oleylamine.[36] When $NaBH_4$ was adding, the color changed appeared while the temperature was just 170 °C. It seems like that the role of $NaBH_4$ was to promote the reduced Ni precursor to Ni phase. To understand the reaction machine, intermediate particles were isolated from the reaction at different temperature. As showed in Fig. S2† and Scheme 1b, without the addition of $NaBH_4$, the nanoparticles go through the Ni precursor –Ni–Ni–P complex – $Ni_{12}P_5$–Ni_2P procedure, consist with the reports.[32,38,39] When $NaBH_4$ was adding, the formation of metal nanoparticles was not found (Fig. 1 and S3†). Amorphous Ni–P intermediates were found until the temperature up to 250 °C. It is noteworthy that all the Ni/P ratios of the Ni–P intermediates were consist with the final phase-pure Ni_2P NCs (Fig. S3, ESI†). These results suggest that $NaBH_4$ does not act as the reducing agent for the transformation of Ni precursor to Ni phase.

Previous study on the Ni–P system revealed that when the P/Ni precursor ratio was excessed to 10, formation of metal NC intermediates were not found and the amorphous Ni–P intermediates lead to the formation of solid metal phosphide NCs.[32] In our experience, the P/Ni precursor ratio was keep at 2. Therefore, we speculate that with the addition of $NaBH_4$, the triphenylphosphine is reacted with $NaBH_4$ firstly. The electrons are transferred from the H^- atoms to the P atoms of triphenylphosphine, leading to P atoms more negative-charged. The negative-charged P would potentially bond with metal atoms, resulting in the formation of amorphous Ni–P intermediates. The adding of $NaBH_4$ has efficiently activated the triphenylphosphine, lowering the thermodynamic barrier for the P–M bond formation and P–C broken. Thus, the reaction temperature for the synthesis of phase-pure metal phosphide NCs can significantly reduce from 330 °C to 250 °C.[38] This low-temperature, facile and economical route to composition controllable multicomponent metal phosphides is expected to have broad applicability.

Crystal structure, morphology and surface chemistry of $Ni_{2-x}Co_xP$ nanoparticles. The compositions of the resulting $Ni_{2-x}Co_xP$ NCs were determined by energy-dispersive X-ray spectroscopy (Fig. S4, ESI†). The Co : Ni : P mole ratios in the

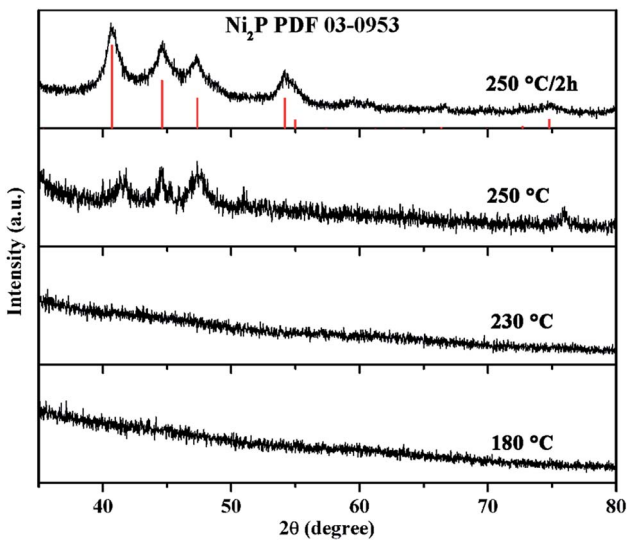

Fig. 1 The XRD patterns Ni_2P nanoparticles isolated from the reaction at different temperatures.

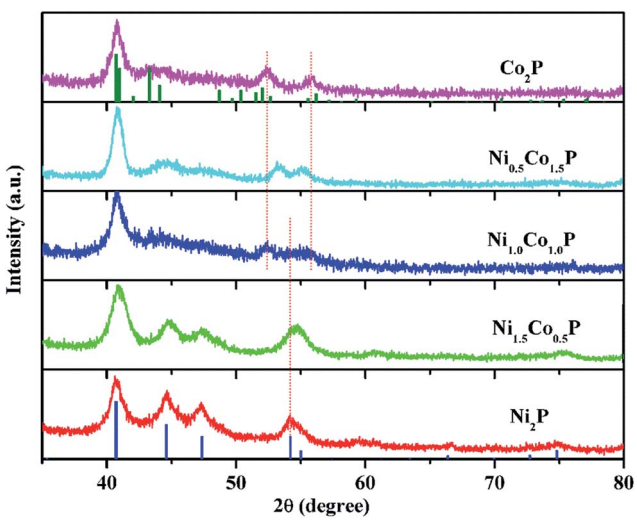

Fig. 2 The XRD patterns of the as-prepared $Ni_{2-x}Co_xP$ NCs.

products are in close agreement with the ratios of the precursors. This indicates that the reactivity of the relative precursors was balanced and the successful formation of compositionally tunable $Ni_{2-x}Co_xP$ NCs was achieved.

Fig. 2 shows the XRD patterns of the as-prepared $Ni_{2-x}Co_xP$ NCs. As for Ni_2P and $Ni_{1.5}Co_{0.5}P$, phases crystallize in the hexagonal Fe_2P structure-type, and all observed XRD peaks are consistent with a JCPDS reference pattern for Ni_2P (card no. 03-0953). For $Ni_{2-x}Co_xP$ NCs with $x \geq 1$, the XRD patterns for the ternary phosphide phases are similar to that of a JCPDS reference pattern for orthorhombic Co_2P (card no. 32-0306). No impurity, such as metal oxide and metal species, is detected by XRD. For the nickel-rich composition, a broad peak near $2\theta = 55^\circ$ is observed, which is corresponding to the overlapping reflections of (300) and (211) planes due to the small size of the particles. As the ratio of Co/Ni increased, two peaks that shift away from each other are appeared, indicating the crystal structure transformation of the as-prepared ternary phosphide NCs. All the XRD patterns of the as-prepared $Ni_{2-x}Co_xP$ NCs are consistent with the result by Brock' group,[39] indicate that the developed protocol is successfully to synthesize $Ni_{2-x}Co_xP$ NCs over the whole range.

The morphology and particle size of the as-prepared $Ni_{2-x}Co_xP$ NCs are analyzed by TEM (Fig. 3). The particles sizes are in the range of 3–11 nm, in consistent with the result from XRD. High-resolution TEM images of the as-prepared $Ni_{2-x}Co_xP$ NCs are shown as insets in each TEM image. The clear lattice fringes for the whole nanocrystals shown in all compositions indicate that these nanoparticles are well crystalline. The EDS, XRD and TEM results indicate that the developed protocol is ideal to synthesize $Ni_{2-x}Co_xP$ NCs with good control of composition.

The surface chemistry of as-prepared $Ni_{2-x}Co_xP$ NCs is investigated by XPS. Fig. 4 shows the detailed XPS spectra of relevant elements with the binding energies. In Fig. 4a, two

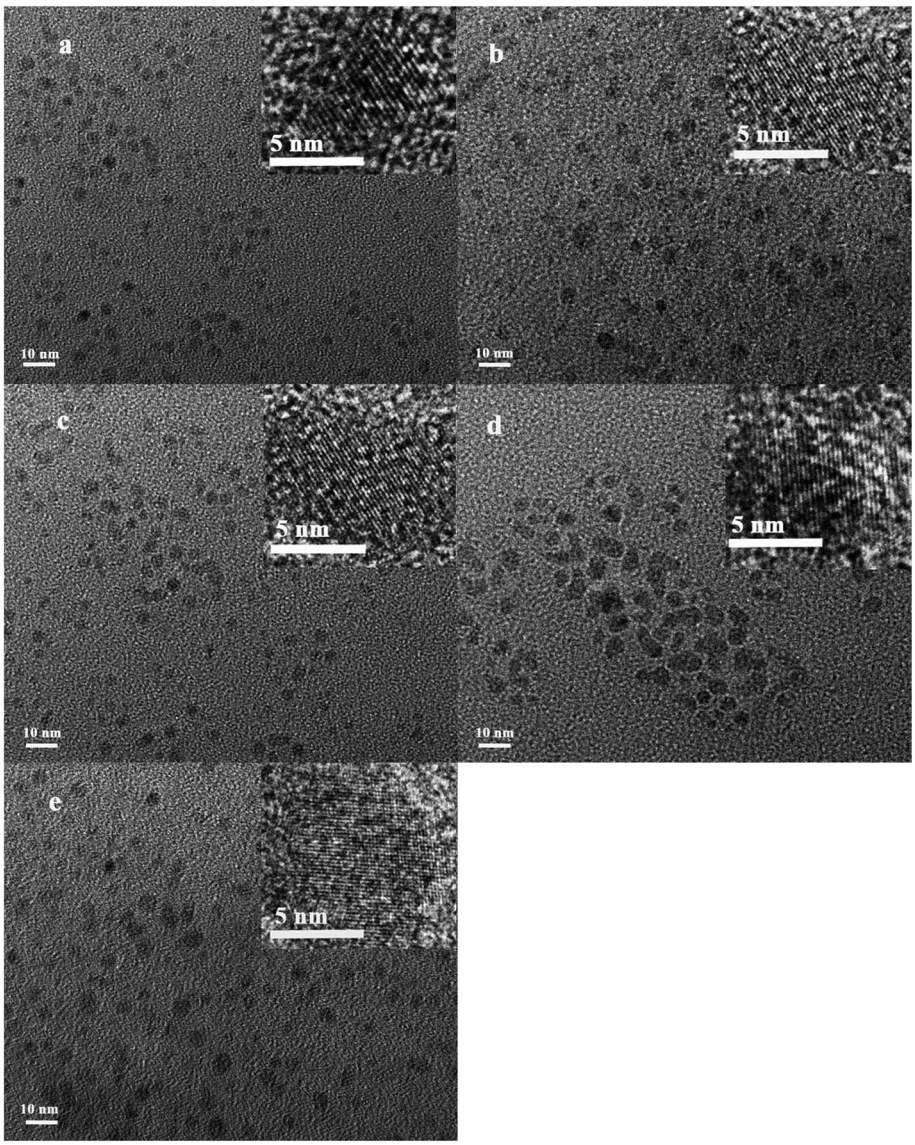

Fig. 3 TEM images for $Ni_{2-x}Co_xP$ nanoparticles (a) Ni_2P; (b) $Ni_{1.5}Co_{0.5}P$; (c) NiCoP; (d) $Ni_{0.5}Co_{1.5}P$; (e) Co_2P. The insets illustrate HRTEM images for each composition showing lattice fringes.

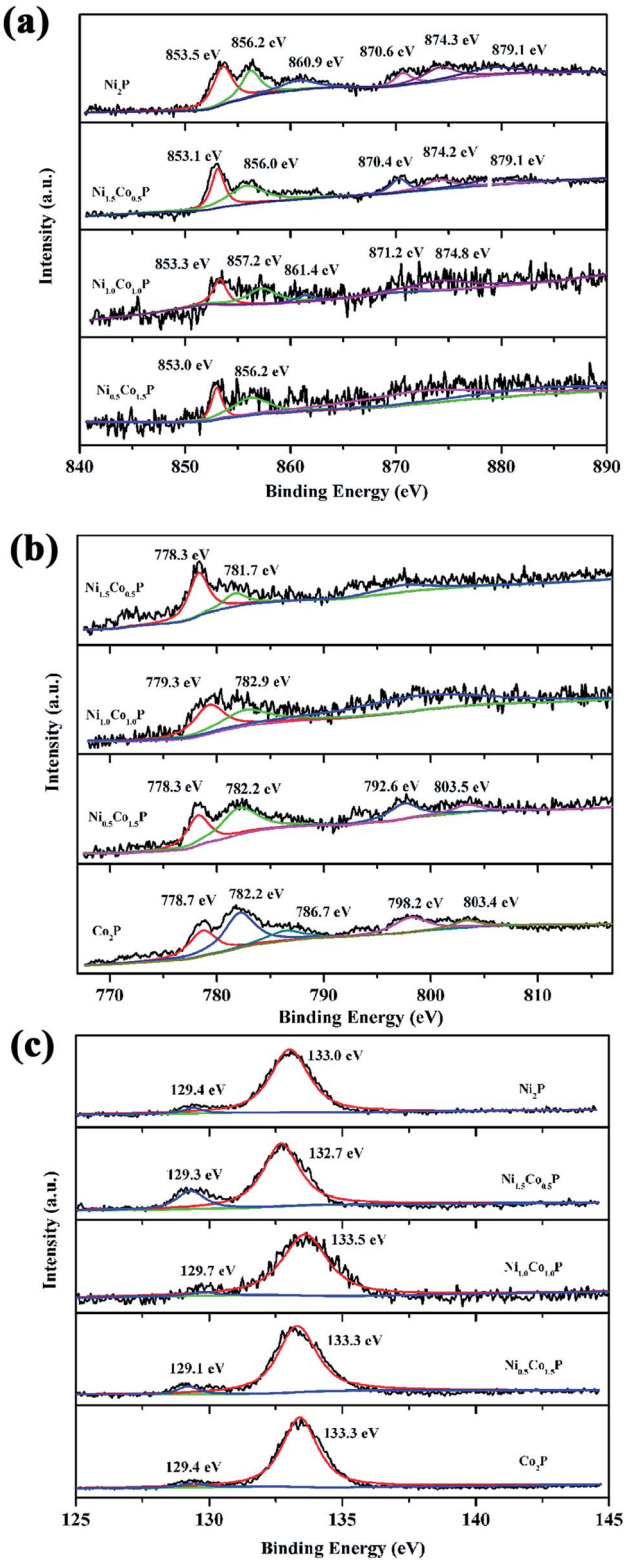

Fig. 4 XPS spectra of as-prepared $Ni_{2-x}Co_xP$ NCs with different compositions.

characteristic peaks around 853.0–853.5 eV and 870.4–871.2 eV are attributed to Ni $2p_{3/2}$ and $2p_{1/2}$ energy levels, respectively, corresponding to $Ni^{\delta+}$ in the Ni–P compound.[15] Another two peaks around 856.0–857.2 eV and 874.2–874.8 eV as well as the satellitic peak at 879.1 eV are assigned to oxidized Ni species. Similarly, for Co element, the Co $2p_{3/2}$ and Co $2p_{1/2}$ peaks around 781.7–782.9 eV and 792.6–798.2 eV as well as the satellitic peak at 803.5 eV can be correlated to the presence of oxidized Co species.[40] The peaks around 778.3–779.3 eV correspond to the Co $2p_{3/2}$ energy level of Co–P species. For P element, the binding energies around 129.1–129.7 eV are ascribed to the P $2p_{3/2}$ and $2p_{1/2}$ doublet of phosphide, while the peaks around 132.7–133.5 eV are correlated to the positive-valence P binding with O species.[22] The appeared oxidize species play great important roles for OER catalysis. The surface compositions of as-prepared $Ni_{2-x}Co_xP$ NCs are also evaluated by XPS (Table S1, ESI†). The surface Co/Ni ratios are slightly larger than those measured by EDS, while the P/(Co + Ni) ratios determined by XPS are in the range 2–4, indicating that the surfaces are Co and P rich.

3.2 Composition dependent catalytic performance for water splitting

OER activities of as-prepared $Ni_{2-x}Co_xP$ NCs. The electrocatalytic OER performances of as-obtained $Ni_{2-x}Co_xP$ NCs are tested by steady-state linear sweep voltammetry (LSV) in basic solutions. Fig. 5a shows the polarization curves of $Ni_{2-x}Co_xP$ NCs with different Co/Ni ratios in 1.0 M KOH. Due to the presence of the oxidation peaks (Ni^{2+}/Ni^{3+}, Co^{2+}/Co^{3+}),[22] the onset potential for the as-prepared catalysts is illegible. As shown in Fig. 5a, Co/Ni composition dependent OER catalysis of $Ni_{2-x}Co_xP$ NCs is observed and $Ni_{1.0}Co_{1.0}P$ NCs show the best catalytic performances due to the synergistic effect. Fig. 5b shows that at current density of 20 mA cm^{-2}, the potentials first decrease and then increase with the Co percentage improve. Fig. 5c shows that the current densities of as-prepared $Ni_{2-x}Co_xP$ NCs catalysts at $\eta = 400$ mV follow a volcano relationship. The overpotential, defined as which the current density reaches 10 mA cm^{-2}, is commonly used as a figure of merit OER catalyst. For as-prepared $Ni_{1.0}Co_{1.0}P$ NCs, the overpotential at a current density of 10 mA cm^{-2} is 0.34 V, which places the $Ni_{1.0}Co_{1.0}P$ NCs catalyst among the top tier of water oxidation catalysts. The volcano trend of catalytic activity was also reflected in the Tafel slopes. As shown in Fig. 5d, the Tafel slopes decrease first and then increase with the Co/Ni ratios. The $Ni_{1.0}Co_{1.0}P$ NCs show the lowest Tafel slopes, implying the most favorable OER catalytic reaction kinetics due to synergistic effect. The integration of two or more metals in a heterogeneous catalyst may induce the presence of multiple valences of the cations with more complex electronic structure and higher electrical conductivity, helps to lower the thermodynamic barrier of a proton-coupled electron pre-equilibrium while facilitating O–O bond formation, thus leading to enhanced catalytic activity. The synergistic effect to reduce the overpotential and Tafel slope has opened a new approach to tune and optimize the electrocatalysis of water oxidize.

HER activities of as-prepared $Ni_{2-x}Co_xP$ NCs. Beside the outstanding OER activities, the $Ni_{2-x}Co_xP$ NCs catalysts are highly active towards HER. Fig. 6 shows the polarization curves of as-prepared $Ni_{2-x}Co_xP$ NCs with different compositions. To

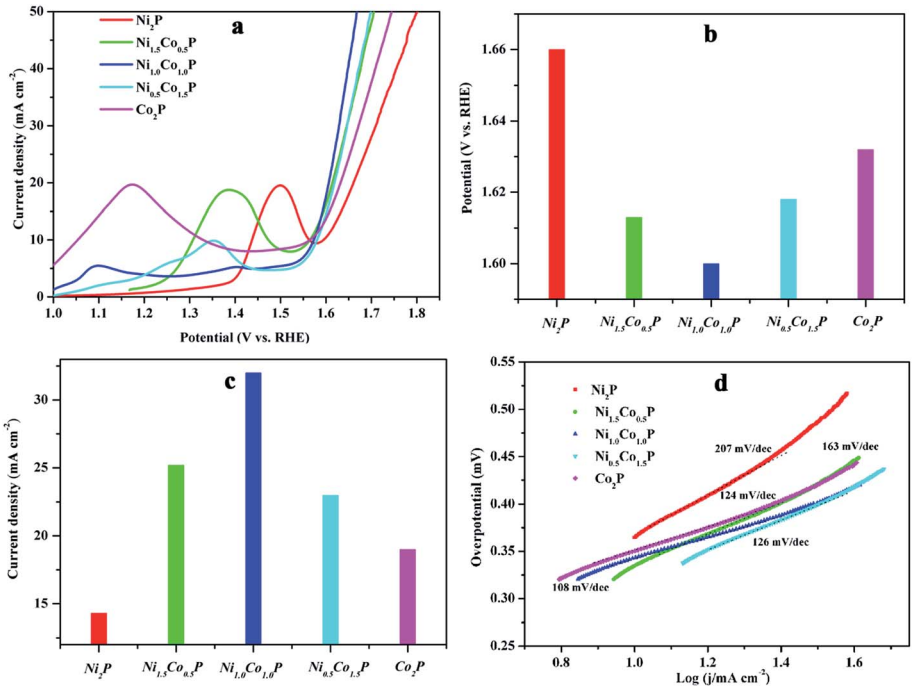

Fig. 5 (a) The polarization curves of $Ni_{2-x}Co_xP$ NCs with different Co/Ni ratios in 1.0 M KOH for OER; (b) the required potentials to achieve a current density of 20 mA cm^{-2} for different $Ni_{2-x}Co_xP$ NCs; (c) current densities at $\eta = 400$ mV; (d) corresponding Tafel plots of $Ni_{2-x}Co_xP$ NCs with different Co/Ni ratios.

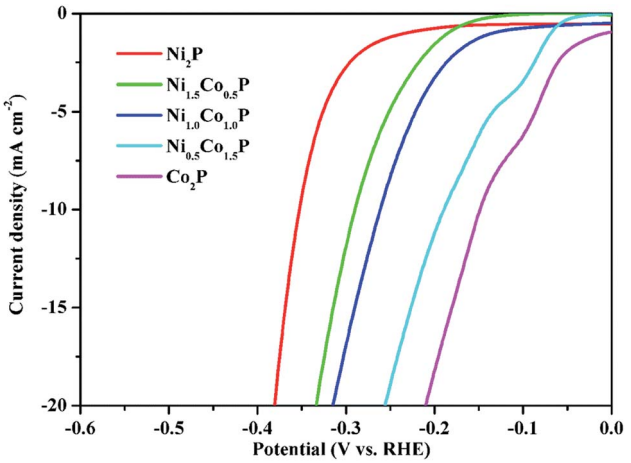

Fig. 6 The polarization curves of as-prepared $Ni_{2-x}Co_xP$ NCs with different compositions in 0.5 M H_2SO_4 for HER.

achieve a current density of 20 mA cm^{-2}, an overpotential (η) of just 184 mV is required for Co_2P, whereas Ni_2P, $Ni_{1.5}Co_{0.5}P$, NiCoP, and $Ni_{0.5}Co_{1.5}P$ require 294, 252, 212, and 202 mV, respectively. It is obvious that the presence of Co is very helpful for lowering the overpotentials. In order to investigate the kinetics of HER electrochemical reaction, Tafel plots for all the catalysts near the onset of substantial cathodic current are measured. Fig. 7 shows the corresponding Tafel plots of $Ni_{2-x}Co_xP$ NCs with different Co/Ni ratios. According to the Tafel equation ($\eta = a + b \log j$, where b is the Tafel slope and j is the current density), the Tafel slopes for Co_2P, $Ni_{0.5}Co_{1.5}P$, NiCoP, $Ni_{1.5}Co_{0.5}P$, and Ni_2P are 55, 59, 63, 93, and 99 mV dec^{-1}, respectively. The observed Tafel slopes indicates that the HER reaction took place *via* a Volmer–Heyrovsky mechanism, which the electrochemical desorption of H_{ads} and H^+ to form hydrogen is the rate limiting step. Generally, a lower slope value indicates more favorable electrochemical reaction kinetic.[3] The Tafel slopes of $Ni_{2-x}Co_xP$ NCs are decreasing with the increasing of Co/Ni ratios, suggesting that the Co ions have stronger electron-donating ability than Ni ions and are more favorable for the H–H bond formation. With increased the Co/Ni ratios, the

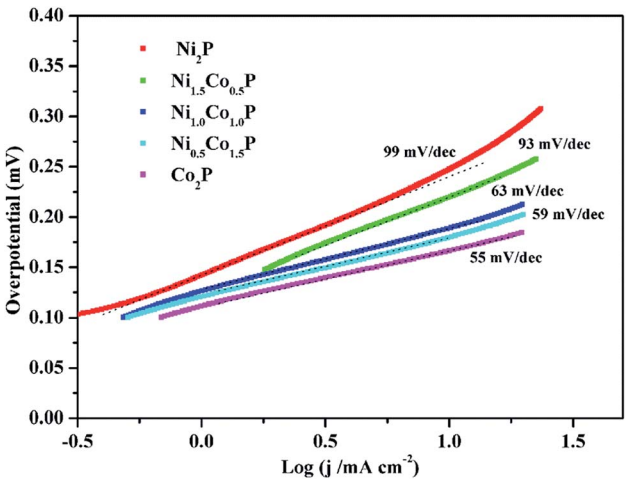

Fig. 7 Tafel plots of $Ni_{2-x}Co_xP$ NCs with different Co/Ni ratios in 0.5 M H_2SO_4 for HER.

activity toward HER is improved, indicating that Co ions act as more favorable hydride acceptor centers than Ni ions in HER catalyze.

In addition to the acidic, the $Ni_{2-x}Co_xP$ NCs also have favorable HER activities in basic media. The representative polarization curves and Tafel plots of $Ni_{2-x}Co_xP$ NCs with different Co/Ni ratios in 1.0 M KOH are shown in Fig. S5.† The overpotential at a current density of mA cm^{-2} for Co_2P, $Ni_{0.5}Co_{1.5}P$, NiCoP, $Ni_{1.5}Co_{0.5}P$, and Ni_2P are 209, 254, 314, 333, and 378 mV, respectively. The HER performance of $Ni_{2-x}Co_xP$ in basic media also strongly depends on Co/Ni ratios and the addition of Co significantly enhances the catalytic performances of Ni_2P. The HER catalytic performances of Co_2P and Ni_2P in both acidic and basic media are comparable with those previously reported non-noble-metal HER electrocatalysts,[9,15,27] demonstrating that the developed protocol is successful to synthesize transition metal phosphides NCs with superior water splitting activity.

4. Conclusion

A facile economical route to synthesize $Ni_{2-x}Co_xP$ NCs with good control of composition is developed. By modulating the Ni/Co precursor ratios, the composition of the resultant NCs could be tuned over the whole range, from Ni_2P to Co_2P. A comprehensive study of the key role of $NaBH_4$ on the metal phosphide NCs formation reveals that $NaBH_4$ can efficiently activate the triphenylphosphine, lowering the thermodynamic barrier for the P–C bond broken and significantly reducing the reaction temperature. The HER catalytic performance of $Ni_{2-x}Co_xP$ in both acidic and basic media are found to be strongly depends on Co/Ni ratios and the addition of Co significantly enhances the catalytic performance. While for OER catalysis, the as-prepared $Ni_{2-x}Co_xP$ NCs follow a volcano trend and $Ni_{1.0}Co_{1.0}P$ NCs exhibit the highest OER catalytic activity with the overpotential of 0.34 V at a current density of 10 mA cm^{-2}. The developed method to prepare component controllable ternary phosphides nanoparticles shines light to the structure–activity study for water splitting catalysts.

Acknowledgements

This work was supported by the National Natural Science Foundation of China (Grants 21427802, 21131002 and 21201075) and the Specialized Research Fund for the Doctoral Program of Higher Education (SRFDP Grant 20110061130005).

References

1 X. Zou and Y. Zhang, *Chem. Soc. Rev.*, 2015, **44**, 5148–5180.
2 P. Xiao, W. Chen and X. Wang, *Adv. Energy Mater.*, 2015, **5**, 1500985.
3 Y. Shi and B. Zhang, *Chem. Soc. Rev.*, 2016, **45**, 1529–1541.
4 Z. Xing, Q. Liu, A. M. Asiri and X. Sun, *Adv. Mater.*, 2014, **26**, 5702–5707.
5 X. Wang, Y. V. Kolen'ko, X. Q. Bao, K. Kovnir and L. Liu, *Angew. Chem.*, 2015, **54**, 8188–8192.
6 S. Cao, Y. Chen, C. J. Wang, P. He and W. F. Fu, *Chem. Comm.*, 2014, **50**, 10427–10429.
7 J.-S. Moon, J.-H. Jang, E.-G. Kim, Y.-H. Chung, S. J. Yoo and Y.-K. Lee, *J. Catal.*, 2015, **326**, 92–99.
8 D. Yang, J. Zhu, X. Rui, H. Tan, R. Cai, H. E. Hoster, D. Y. Yu, H. H. Hng and Q. Yan, *ACS Appl. Mater. Interfaces*, 2013, **5**, 1093–1099.
9 J. Ryu, N. Jung, J. H. Jang, H.-J. Kim and S. J. Yoo, *ACS Catal.*, 2015, **5**, 4066–4074.
10 L.-A. Stern, L. Feng, F. Song and X. Hu, *Energy Environ. Sci.*, 2015, **8**, 2347–2351.
11 R. Ye, P. Del Angel-Vicente, Y. Liu, M. J. Arellano-Jimenez, Z. Peng, T. Wang, Y. Li, B. I. Yakobson, S. H. Wei, M. J. Yacaman and J. M. Tour, *Adv. Mater.*, 2016, **28**, 1427–1432.
12 C. Y. Son, I. H. Kwak, Y. R. Lim and J. Park, *Chem. Comm.*, 2016, **52**, 2819–2822.
13 X. Yang, A. Y. Lu, Y. Zhu, S. Min, M. N. Hedhili, Y. Han, K. W. Huang and L. J. Li, *Nanoscale*, 2015, **7**, 10974–10981.
14 Y. Pan, W. Hu, D. Liu, Y. Liu and C. Liu, *J. Mater. Chem. A*, 2015, **3**, 13087–13094.
15 Y. Pan, Y. Liu, J. Zhao, K. Yang, J. Liang, D. Liu, W. Hu, D. Liu, Y. Liu and C. Liu, *J. Mater. Chem. A*, 2015, **3**, 1656–1665.
16 H. Du, Q. Liu, N. Cheng, A. M. Asiri, X. Sun and C. M. Li, *J. Mater. Chem. A*, 2014, **2**, 14812.
17 Y. Pan, Y. Liu and C. Liu, *J. Power Sources*, 2015, **285**, 169–177.
18 Y. Pan, N. Yang, Y. Chen, Y. Lin, Y. Li, Y. Liu and C. Liu, *J. Power Sources*, 2015, **297**, 45–52.
19 Z. Huang, Z. Chen, Z. Chen, C. Lv, M. G. Humphrey and C. Zhang, *Nano Energy*, 2014, **9**, 373–382.
20 B. You, N. Jiang, M. Sheng, M. W. Bhushan and Y. Sun, *ACS Catal.*, 2016, **6**, 714–721.
21 M. Liu and J. Li, *ACS Appl. Mater. Interfaces*, 2016, **8**, 2158–2165.
22 Z. Zhang, J. Hao, W. Yang and J. Tang, *RSC Adv.*, 2016, **6**, 9647–9655.
23 C. G. Read, J. F. Callejas, C. F. Holder and R. E. Schaak, *ACS Appl. Mater. Interfaces*, 2016, **8**, 12798–12803.
24 L. Feng, H. Vrubel, M. Bensimon and X. Hu, *Phys. Chem. Chem. Phys.*, 2014, **16**, 5917–5921.
25 M. H. Hansen, L. A. Stern, L. Feng, J. Rossmeisl and X. Hu, *Phys. Chem. Chem. Phys.*, 2015, **17**, 10823–10829.
26 J. Kibsgaard, C. Tsai, K. Chan, J. D. Benck, J. K. Nørskov, F. Abild-Pedersen and T. F. Jaramillo, *Energy Environ. Sci.*, 2015, **8**, 3022–3029.
27 A. Mendoza-Garcia, D. Su and S. Sun, *Nanoscale*, 2016, **8**, 3244–3247.
28 J. F. Callejas, C. G. Read, C. W. Roske, N. S. Lewis and R. E. Schaak, *Chem. Mater.*, 2016, **28**, 6017–6044.
29 M. Sun, H. Liu, J. Qu and J. Li, *Adv. Energy Mater.*, 2016, **6**, 1600087.
30 Y. Deng, Y. Zhou, Y. Yao and J. Wang, *New J. Chem.*, 2013, **37**, 4083.
31 L. Guo, Y. Zhao and Z. Yao, *Dalton Trans.*, 2016, **45**, 1225–1232.

32 J. Wang, A. C. Johnston-Peck and J. B. Tracy, *Chem. Mater.*, 2009, **21**, 4462–4467.
33 G. H. Layan Savithra, E. Muthuswamy, R. H. Bowker, B. A. Carrillo, M. E. Bussell and S. L. Brock, *Chem. Mater.*, 2013, **25**, 825–833.
34 A. Hitihami-Mudiyanselage, M. P. Arachchige, T. Seda, G. Lawes and S. L. Brock, *Chem. Mater.*, 2015, **27**, 6592–6600.
35 S. E. Habas, F. G. Baddour, D. A. Ruddy, C. P. Nash, J. Wang, M. Pan, J. E. Hensley and J. A. Schaidle, *Chem. Mater.*, 2015, **27**, 7580–7592.
36 D.-H. Ha, L. M. Moreau, C. R. Bealing, H. Zhang, R. G. Hennig and R. D. Robinson, *J. Mater. Chem.*, 2011, **21**, 11498.
37 W. Yang, Y. Huang, J. Fan, Y. Yu, C. Yang and H. Li, *Nanoscale*, 2016, **8**, 4898–4902.
38 H. Song, M. Dai, H.-L. Song, X. Wan, X.-W. Xu and Z.-S. Jin, *J. Mol. Catal. A: Chem.*, 2014, **385**, 149–159.
39 D. R. Liyanage, S. J. Danforth, Y. Liu, M. E. Bussell and S. L. Brock, *Chem. Mater.*, 2015, **27**, 4349–4357.
40 Y. Feng, X. Y. Yu and U. Paik, *Chem. Comm.*, 2016, **52**, 1633–1636.